Bulk-like Magnetic Moment of Epitaxial Two-dimensional Superlattices

Jiabao Sun,[1] Shanshan Liu,[2,3] Faxian Xiu,[2,3] Wenqing Liu,[1*]

[1] Department of Electronic Engineering, Royal Holloway University of London, Egham TW20 0EX, UK
[2] State Key Laboratory of Surface Physics and Department of Physics, Fudan University, Shanghai 200433, China
[3] Institute for Nanoelectronic Devices and Quantum Computing, Fudan University, Shanghai 200433, China
* Email: wenqing.liu@rhul.ac.uk

Over the past four years, the magnetism of 2D magnets has been extensively studied by the full arsenal of probing techniques. 2D magnets can be incorporated to form heterostructures with clean and sharp interfaces, which gives rise to exotic phenomena as a result of the interfacial proximity effect. Here we report a detailed study of the spin (m_s) and orbital (m_l) moments of an epitaxial $(CrSb/Fe_3GeTe_2)_6$ superlattice. The synchrotron-radiation based x-ray magnetic circular dichroism (XMCD) technique was performed to probe the microscopic magnetic properties of the superlattices in an elemental resolved manner. We unambiguously obtained a bulk-like moment of Fe_3GeTe_2 i.e., m_s = 1.58 ± 0.2 μ_B/Fe and m_l = 0.22 ± 0.02 μ_B/Fe. Future works to explore the tuning of the spin polarized band structure of 2D ferromagnetic superlattices will be of great interest and can have strong implications for both fundamental physics and the emerging spintronics technology.

***Index Terms*—2D magnets, superlattice, epitaxial thin films, magnetic moment, x-ray magnetic circular dichroism (XMCD), spintronics.**

I. Introduction

The van der Waals (vdWs) crystals or two dimensional (2D) materials, have been widely studied since graphene, the first 2D material, was isolated in 2004 [1], [2]. The research into 2D materials has rapidly covered various fields ranging from semiconductors to highly correlated materials and superconductors [3]. Recent research has focused on the magnetism in 2D materials. The Mermin–Wagner theorem [4] demonstrates that the thermal fluctuation in isotropic 2D systems can destroy long-range magnetic order at any finite temperature (T > 0), which is due to the presence of gapless spin-wave excitations in isotropic systems with continuous symmetry. The magnetocrystalline anisotropy can open the magnon excitation gap in the spin-wave spectrum of 2D system to maintain long-range magnetic order at non-zero temperatures. In 2017, the 2D ferromagnetic order was firstly demonstrated in two vdWs insulators, $Cr_2Ge_2Te_6$ [5] and CrI_3 [6], with the strong perpendicular anisotropy compensating the effect of thermal fluctuation to stabilize magnetic order in 2D systems. One year later, the itinerant 2D ferromagnetism was reported in Fe_3GeTe_2 monolayers [7]–[9]. The family of 2D magnets has been further expanded, e.g., $MnSe_2$ [10], $CrCl_3$ [11], and $CrBr_3$ [12], and their magnetic properties have been extensively studied using superconducting quantum interference device vibrate sample magnetometer (SQUID-VSM) [10], tunneling magnetoresistance effect (TMR) measurement [11] and scanning tunneling microscope (STM) [12], respectively. The discovered vdWs magnets offer a great platform to study 2D ferromagnetism and have exhibited great potential in developing spintronic devices by manipulating both spin and charge degrees of freedom [13].

Among the discovered 2D magnetic materials, Fe_3GeTe_2 has become a promising candidate for 2D spintronics because of its relatively high Curie temperature (T_C = ~ 220 K) and strong perpendicular anisotropy [14]–[18]. Strong electron correlation effects have been predicated in Fe_3GeTe_2 single crystals [19]. Fe_3GeTe_2 has layered hexagonal crystal structure where the covalent bonded metallic Fe_3Ge slabs are sandwiched by Te layers to hold the whole structure via vdWs force as shown in Fig. 1a. There are two nonequivalent Fe sites in Fe_3Ge slabs, Fe^{I} and Fe^{II}. Two Fe^{I} atoms are located at the center of each hexagonal plaquettes and separated by the covalent bonded Fe^{II}-Ge honeycomb slab that determines the whole crystalline symmetry. The parallel coupled spins of Fe^{I} and Fe^{II} ions have been experimentally confirmed by neutron diffraction [16]. To achieve electric field switchable spintronic devices by Fe_3GeTe_2, a strong spin-orbital coupling (SOC) or at least an unquenched orbital moment is needed in itinerant magnetic system [20]. Various techniques, including SQUID-VSM [14]–[17], [21]–[25], x-ray magnetic circular dichroism (XMCD) [19], [26], and neutron diffraction [16], [24] have been used to study the atomic-scale magnetic moment of Fe_3GeTe_2. The calculations of the system have been carried out by local density approximation (LDA) [27], LDA+U [18], and LDA combine with dynamical mean-field theory (LDA+DMFT) [19]. The total magnetic moments (m_{total}) varies from 1.8 μ_B/Fe by Verchenko et al. using SQUID-VSM [24], to 1.63 μ_B/Fe by Chen et al. with SQUID-VSM [15] and 1.58 μ_B/Fe by Zhu et al. using XMCD [19], and all the way down to approximately 1.2 ± 0.03 μ_B/Fe by Deiseroth et al. [14], and Liu et al. [21] using SQUID-VSM. The theoretical result varies from 1.68 μ_B/Fe by Zhu et al. [19], to 1.57 μ_B/Fe by Lin et al. [27], and down to 1.48 μ_B/Fe by Zhuang et al. [18].

Recent attentions have focused on controlling and manipulating the magnetic anisotropy [28] and T_C [8], [16], [21] of Fe_3GeTe_2 using external perturbations, such as doping [16], [21], [28] and gating [8]. By their nature, 2D magnets can be stacked to form vdWs heterostructures with clean and sharp interface, and negligible lattice mismatch. This superiority gives rise to exotic phenomena in 2D magnetic

films as a result of the interfacial magnetic proximity effect without the deleterious effect in conventional magnetic heterostructures. The magnetic proximity effect in vdWs heterostructures was firstly studied in graphene/$Y_3Fe_5O_{12}$ [29] and graphene/EuS [30] heterostructures to form magnetic order in graphene. In 2017, the T_C = 54 K of Cr-(Bi, Sb)$_2$Se$_3$ was achieved in a (Cr-(Bi, Sb)$_2$Se$_3$/CrSb) heterostructure, and was enhanced to ~90 K by stacking into a ten period superlattice [31].

Very recently, we have demonstrated the first inch-scale epitaxial two-dimensional ferromagnetic superlattices $(CrSb/Fe_3GeTe_2)_3$, in which Fe_3GeTe_2 shows a significantly reduced spin moment (m_s = 1.05 μ_B/atom) [26] comparing to bulk Fe_3GeTe_2 [19]. The CrSb film is a high Néel temperature (T_N = ~ 700 K) antiferromagnetic material with hexagonal symmetry [32]. It is one of the few antiferromagnets that is lattice-matched with Fe_3GeTe_2 films [26]. Here we report a further study of the epitaxial $(CrSb/Fe_3GeTe_2)_6$ superlattices using the x-ray magnetic circular dichroism (XMCD) technique. The superlattices were grown by molecular beam epitaxy (MBE) and was measured with magnetotransport techniques. The anomalous Hall effect show a near-square-shaped hysteresis loop with large coercivity (1.12 T) along c axis, i.e., strong perpendicular anisotropy. The x-ray absorption spectroscopy (XAS) spectra at Fe $L_{2,3}$ show good agreement with that of bulk Fe_3GeTe_2 [19]. By applying sum rules, we obtained a bulk-like magnetic moments of Fe_3GeTe_2 (m_s = 1.58 ± 0.2 μ_B/Fe & m_l = 0.22 ± 0.02 μ_B/Fe). The sizable spin and orbital moments of Fe_3GeTe_2 layers make the epitaxial $(CrSb/Fe_3GeTe_2)_n$ superlattices a promising candidate for the development of the next generation energy efficient spintronic devices.

II. EXPERIMENTAL DETAILS

The $(CrSb/Fe_3GeTe_2)_6$ superlattices were epitaxially grown using a Perkin Elmer 430 MBE system on sapphire (0001) with a base pressure of 10^{-9} Torr. The 4-layer (3.2 nm) ferromagnetic (FM) Fe_3GeTe_2 thin films were grown at a substrate temperature (T_s) of ~310℃. Fe (99.99%), Ge (99.999%) and Te (99.999%) were co-evaporated from Knudsen cells with the source temperatures of 1165℃, 1020℃ and 285℃, respectively. The substrate temperature was subsequently reduced to 280℃ for 1.6 nm CrSb films growth, which was carried out on the Fe_3GeTe_2 layers by evaporating Cr (99.99%) and Sb (99.999%) with cell temperatures of 1180℃ and 400℃, respectively. 4 nm Al capping layers were in-situ evaporated on the top of superlattices to protect them from oxidation in ambient environment. The thickness of thin films were determined by transmission electron microscope as published before [26].

The global magnetic properties of $(CrSb/Fe_3GeTe_2)_6$ superlattices were investigated by transport measurement via anomalous Hall effect (AHE) using a Quantum Design Physical Properties Measurement system. The $(CrSb/Fe_3GeTe_2)_6$ superlattices were confined into a Hall-bar geometry with a size of 1.5 × 2 mm^2 as shown in inset of Fig. 1c. The data were collected with a lock-in amplifiers (Stanford Research 830, Stanford Research Systems, Sunnyvale, CA, USA). The field dependent Hall resistance (R_{xy}) measurements (R-H) of $(CrSb/Fe_3GeTe_2)_6$ superlattices were carried out under an out-of-plane magnetic field and repeated at the elevated temperatures ranging from 2.5 K to 250 K.

The synchrotron-based XAS and XMCD technique were performed at Fe and Cr $L_{2,3}$ at Beamline I10 of the Diamond Light Source to unambiguously determine magnetic moments of the superlattices in an elemental resolved manner. Oppositely circular polarized x-rays with 100% degree of polarization were used successively to resolve XMCD signals from each of the magnetic elements, in which the beam was applied in normal incidence with respect to the film plane and in parallel with external magnetic fields, as shown in Figure 2a. The temperature dependent measurements were performed from 3 K to 150 K under an applied field 5 T (out-of-plane) with total electron yield (TEY) mode. The XMCD was obtained by subtracting the two XAS spectra, (σ^- - σ^+), achieved by switching the XAS helicity at APPLE II undulators [33], [34]. In order to remove the non-magnetic signal due to photoexcitation into continuum states, an arctangent step function was fitted as threshold and subtracted from XAS spectra [35]. The spin and orbital moments, i.e., m_s and m_l, were calculated by applying sum rules, i.e., Eq. 1, on the integration of total XAS and XMCD spectra at Fe and Cr $L_{2,3}$ edges.

$$m_s = -n_h \frac{6\int_{L_3}(\sigma^- - \sigma^+)dE - 4\int_{L_{2,3}}(\sigma^- - \sigma^+)dE}{\int_{L_{2,3}}(\sigma^- + \sigma^+)dE} - \langle T_z \rangle$$
$$m_l = -\frac{4}{3} n_h \frac{\int_{L_{2,3}}(\sigma^- - \sigma^+)dE}{\int_{L_{2,3}}(\sigma^- + \sigma^+)dE} \quad (1)$$

where E, $\langle T_z \rangle$ and n_h, is the photon energy, the magnetic dipole term, and the 3d band holes, respectively. The n_h is 4 for Fe [19] and 7 for Cr [36]. The contribution of magnetic dipole term $\langle T_z \rangle$ of 3d electrons is typically smaller than 5% and therefore neglected in this work.

III. RESULTS AND DISCUSSIONS

The hysteresis loops of $(CrSb/Fe_3GeTe_2)_6$ superlattices at 2.5 – 250 K are shown in Fig. 1b, in which the value of R_{xy} is proportional to the global magnetization. The nearly rectangular loop and the 1.12 T coercive field (H_c) along c-axis (Fig. 1b) prove the strong perpendicular anisotropy of the superlattices, which is consistent with the bulk Fe_3GeTe_2 [14]–[17], [21]–[25]. The saturation field of the superlattices is nearly 3.5 T at 2.5 K whilst that of bulk Fe_3GeTe_2 is typically small (< 0.5 T) [15], [22]. The terraced features, double-switching features, were observed near zero field at 2.5 K and persists to 25 K. This double switching feature occurs generally at the interfaces of FM/AFM/FM trilayers due to the FM-AFM interfacial pinning effect [26], [31], [37]. In addition, an enhanced magnetic order is demonstrated by the large $\mu_0 H_c$ = 1.12 T of the $(CrSb/Fe_3GeTe_2)_6$ superlattices at 2.5 K (Fig. 1c), which is significantly larger than that of bulk Fe_3GeTe_2 ($\mu_0 H_c$ = 0.02 T) [16], [18], [19], [23]. As the

temperature increases, the H_c decreases and approaches 3 mT at 230 K (Fig. 1c). The H_c of the superlattices vanishes at 250 K which is close to T_C of the bulk Fe_3GeTe_2 i.e. 220 K [14]–[18].

FIG. 1 HERE

Figure 2b and 2c show typical pairs of XAS and XMCD spectra of the $(CrSb/Fe_3GeTe_2)_6$ superlattices obtained at 3 K-150 K. The XAS of Fe $L_{2,3}$ edges well resembles that of bulk Fe_3GeTe_2 [19], and that of Cr show multiple structures for both spin-orbit split core levels. The strongly dichroic spectra of Fe and Cr persist up to 150 K, indicating the ferromagnetic coupling between the Fe_3GeTe_2 and the CrSb layers in the superlattices. The larger dichroism (thus larger magnetic moments) at Cr $L_{2,3}$ edges was observed at 150 K compared to that of $(CrSb/Fe_3GeTe_2)_3$ superlattices [26], which is generally obtained with increasing number of periods (n) of magnetic superlattices [31], [38]. The sum rules derived spin and orbital moment of the $(CrSb/Fe_3GeTe_2)_6$ superlattices are m_s = 1.58 ± 0.2 μ_B/atom and m_l = 0.22 ± 0.02 μ_B/atom for the Fe and m_s = 0.94 ± 0.09 μ_B/atom and m_l = -0.29 ± 0.03 μ_B/atom for the Cr, respectively (see experimental details). The XMCD derived m_s and m_l of Cr have opposite signs. Figure 2d presents the temperature dependent m_s and m_l for Fe and Cr at 3 K-150 K, respectively, which exhibit the Curie-like trend.

FIG. 2 HERE

There has been a big variation in the reported magnetic moments of Fe_3GeTe_2 systems. With the neutron powder diffraction measurement, Verchenko et al. [24] obtained 1.8 μ_B/Fe of bulk Fe_3GeTe_2, which is the highest saturation moment of single crystal Fe_3GeTe_2 reported so far. A slightly reduced moment of 1.63 μ_B/Fe was obtained using VSM in Fe_3GeTe_2 single crystals by Chen et al. [15]. Zhu et al. [19] performed XMCD measurements of single crystal Fe_3GeTe_2 and obtained m_l = 0.1 μ_B/Fe and m_s = 1.48 μ_B/Fe at 45 K. This is consistent with our results at 50 K. Further smaller magnetic moment of bulk Fe_3GeTe_2, i.e. 1.37 μ_B/Fe was reported by Wang et al. [22] using SQUID-VSM, and 1.31 μ_B/Fe and 1.11 μ_B/Fe by May et al. using neutron diffraction [16]. The later has been attributed to the decreased Fe composition during the self-flux growth process of Fe_3GeTe_2. Similarly Ding et al. [25] reported 1.08 μ_B/Fe of self-flux grown single crystals Fe_3GeTe_2. The epitaxial grown Fe_3GeTe_2 thin films were firstly reported by Liu et al. [21] in 2017. The authors obtained 1.23 μ_B/Fe in a wafer-scale 8 nm Fe_3GeTe_2/Al_2O_3 (0001) film using SQUID-VSM [21]. In our recent work of the epitaxial $(CrSb/Fe_3GeTe_2)_n$ superlattices, 1.21 μ_B/Fe was obtained when n=3 [26].

The variation also exist in theorical works. The calculated m_l = 0.063 μ_B/Fe and m_s = 1.58 μ_B/Fe by Zhu et al. using the LDA+DMFT are consistent with the results by them using XMCD measurement [19], which also agree well with our results. A slightly decreased magnetic moment of 1.57 μ_B/Fe was obtained by Lin et al using LDA [27]. Zhuang et al. reported 1.48 μ_B/Fe of bulk Fe_3GeTe_2 using LDA+U [18]. Table 1 summarizes some of the experimental and theoretical data for the controversy. The magnetic moment in our work (the first line of the table) exhibits a bulk-like magnetic moment of Fe_3GeTe_2 in the epitaxial $(CrSb/Fe_3GeTe_2)_6$ superlattices. The large ratio m_l/m_s = 0.14 confirms the enhanced m_l of Fe_3GeTe_2 in the superlattices compared to that of bulk Fe_3GeTe_2 [19].

TABLE I HERE

The variation of magnetic moments between single crystals and epitaxial growth films is nearly 30%, which is usually from the less symmetry of Fe_3GeTe_2 at the surface and interface of epitaxial Fe_3GeTe_2/Al_2O_3. Due to the extremely large thickness of Fe_3GeTe_2 single crystal, the bulk magnetism can be less impacted by the defect at the surfaces. The off stoichiometry also plays a role in reducing saturation magnetization of bulk and the epitaxial grown Fe_3GeTe_2. By epitaxially growing $(CrSb/Fe_3GeTe_2)_6$ superlattices, the moment of Fe_3GeTe_2 has been successfully built up and is comparable to that of Fe_3GeTe_2 crystals [24]. The enhanced magnetic moment of Fe_3GeTe_2 originates from the interfacial magnetic proximity effect of CrSb layers. Therefore, our results indicate that the epitaxial $(CrSb/Fe_3GeTe_2)_6$ superlattices can effectively avoid the drawbacks of epitaxial thin films and obtain bulk-like moment.

IV. Conclusion

In conclusion, we have performed magnetotransport and XMCD measurements of the epitaxial $(CrSb/Fe_3GeTe_2)_6$ superlattices on Al_2O_3 (0001). High quality of XAS and XMCD spectra were obtained and carefully analyzed with the sum rules. The strongly dichroic spectra of Fe and Cr persist up to 150 K, indicating the ferromagnetic coupling between the Fe_3GeTe_2 and the CrSb. The sum-rules-derived spin and orbital moment of the $(CrSb/Fe_3GeTe_2)_6$ superlattices are m_s = 1.58 ± 0.2 μ_B/atom and m_l = 0.22 ± 0.02 μ_B/atom for the Fe and m_s = 0.94 ± 0.09 μ_B/atom and m_l = -0.29 ± 0.03 μ_B/atom for the Cr, respectively. Regardless the large H_c (1.12 T), a bulk like moment of Fe_3GeTe_2 was observed in the $(CrSb/Fe_3GeTe_2)_6$ superlattices. In addition, the unquenched m_l of Fe and Cr suggest sizable spin-orbital coupling in this system. Our work demonstrates the first inch-scale epitaxial 2D magnet thin films showing a bulk-like moment. This makes metallic Fe_3GeTe_2 a promising candidate for realizing the whole electrical spintronic operations.

Acknowledgment

This work is supported by UK EPSRC (EP/S010246/1), Royal Society (IEC\NSFC\181680), and Leverhulme trust (LTSRF1819\15\12). Diamond Light Source is acknowledged to Beamline I10 under proposal SI20748.

References

[1] K. S. Novoselov, “Electric Field Effect in Atomically Thin Carbon

Films," *Science*, vol. 306, no. 5696, pp. 666–669, Oct. 2004.
[2] K. S. Novoselov *et al.*, "Two-dimensional atomic crystals," 2005.
[3] K. S. Novoselov, A. Mishchenko, A. Carvalho, and A. H. Castro Neto, "2D materials and van der Waals heterostructures," *Science*, vol. 353, no. 6298, 2016.
[4] N. D. Mermin and H. Wagner, "Absence of ferromagnetism or antiferromagnetism in one- or two-dimensional isotropic Heisenberg models," *Phys. Rev. Lett.*, vol. 17, no. 22, pp. 1133–1136, Nov. 1966.
[5] C. Gong *et al.*, "Discovery of intrinsic ferromagnetism in two-dimensional van der Waals crystals," *Nature*, vol. 546, no. 7657, pp. 265–269, 2017.
[6] B. Huang *et al.*, "Layer-dependent ferromagnetism in a van der Waals crystal down to the monolayer limit.," *Nature*, vol. 546, no. 7657, pp. 270–273, 2017.
[7] Z. Fei *et al.*, "Two-dimensional itinerant ferromagnetism in atomically thin Fe3GeTe2," *Nat. Mater.*, vol. 17, no. 9, pp. 778–782, 2018.
[8] Y. Deng *et al.*, "Gate-tunable room-temperature ferromagnetism in two-dimensional Fe3GeTe2," *Nature*, vol. 563, no. 7729, pp. 94–99, Nov. 2018.
[9] K. Kim *et al.*, "Large anomalous Hall current induced by topological nodal lines in a ferromagnetic van der Waals semimetal," *Nat. Mater.*, vol. 17, no. 9, pp. 794–799, 2018.
[10] D. J. O'Hara *et al.*, "Room Temperature Intrinsic Ferromagnetism in Epitaxial Manganese Selenide Films in the Monolayer Limit," *Nano Lett.*, vol. 18, no. 5, pp. 3125–3131, 2018.
[11] X. Cai *et al.*, "Atomically Thin CrCl3: An in-Plane Layered Antiferromagnetic Insulator," *Nano Lett*, vol. 19, p. 35, 2019.
[12] W. Chen *et al.*, "Direct observation of van der Waals stacking–dependent interlayer magnetism," *Science*, vol. 366, no. 6468, pp. 983–987, Nov. 2019.
[13] X. Lin, W. Yang, K. L. Wang, and W. Zhao, "Two-dimensional spintronics for low-power electronics," *Nat. Electron.*, vol. 2, no. July, pp. 22–24, 2019.
[14] H.-J. Deiseroth, K. Aleksandrov, C. Reiner, L. Kienle, and R. K. Kremer, "Fe3GeTe2 and Ni3GeTe2 – Two New Layered Transition-Metal Compounds: Crystal Structures, HRTEM Investigations, and Magnetic and Electrical Properties," *Eur. J. Inorg. Chem.*, vol. 2006, no. 8, pp. 1561–1567, Apr. 2006.
[15] B. Chen *et al.*, "Magnetic properties of layered itinerant electron ferromagnet Fe3GeTe2," *J. Phys. Soc. Japan*, vol. 82, no. 12, pp. 1–7, 2013.
[16] A. F. May, S. Calder, C. Cantoni, H. Cao, and M. A. McGuire, "Magnetic structure and phase stability of the van der Waals bonded ferromagnet Fe3-xGeTe2," *Phys. Rev. B*, vol. 93, no. 1, p. 14411, 2016.
[17] J. Yi *et al.*, "Competing antiferromagnetism in a quasi-2D itinerant ferromagnet: Fe 3 GeTe 2," *2D Mater.*, vol. 4, no. 1, p. 011005, Nov. 2016.
[18] H. L. Zhuang, P. R. C. Kent, and R. G. Hennig, "Strong anisotropy and magnetostriction in the two-dimensional Stoner ferromagnet Fe3GeTe2," *Phys. Rev. B*, vol. 93, no. 13, p. 134407, 2016.
[19] J. X. Zhu *et al.*, "Electronic correlation and magnetism in the ferromagnetic metal Fe3GeTe2," *Phys. Rev. B*, vol. 93, no. 14, p. 144404, 2016.
[20] W. G. Wang, M. Li, S. Hageman, and C. L. Chien, "Electric-field-assisted switching in magnetic tunneljunctions," *Nat. Mater.*, vol. 11, no. 1, pp. 64–68, Nov. 2012.
[21] S. Liu *et al.*, "Wafer-scale two-dimensional ferromagnetic Fe3GeTe2 thin films grown by molecular beam epitaxy," *npj 2D Mater. Appl.*, vol. 1, no. 1, p. 30, 2017.
[22] Y. Wang *et al.*, "Anisotropic anomalous Hall effect in triangular itinerant ferromagnet Fe3GeTe2," *Phys. Rev. B*, vol. 96, no. 13, pp. 1–6, 2017.
[23] Y. Liu, V. N. Ivanovski, and C. Petrovic, "Critical behavior of the van der Waals bonded ferromagnet Fe3-xGeTe2," *Phys. Rev. B*, vol. 96, no. 14, p. 144429, 2017.
[24] V. Y. Verchenko, A. A. Tsirlin, A. V. Sobolev, I. A. Presniakov, and A. V. Shevelkov, "Ferromagnetic Order, Strong Magnetocrystalline Anisotropy, and Magnetocaloric Effect in the Layered Telluride Fe 3−δ GeTe 2," *Inorg. Chem.*, vol. 54, no. 17, pp. 8598–8607, Sep. 2015.
[25] B. Ding *et al.*, "Observation of Magnetic Skyrmion Bubbles in a van der Waals Ferromagnet Fe3GeTe2," *Nano Lett.*, vol. 20, no. 2, pp. 868–873, 2020.
[26] S. Liu *et al.*, "Two-dimensional ferromagnetic superlattices," *Natl. Sci. Rev.*, vol. 7, no. 4, pp. 745–754, Apr. 2020.
[27] X. Lin and J. Ni, "Layer-dependent intrinsic anomalous Hall effect in Fe3GeTe2," *Phys. Rev. B*, vol. 100, no. 8, p. 85403, 2019.
[28] S. Y. Park *et al.*, "Controlling the Magnetic Anisotropy of the van der Waals Ferromagnet Fe3GeTe2 through Hole Doping," *Nano Lett.*, p. A-F, Dec. 2019.
[29] Z. Wang, C. Tang, R. Sachs, Y. Barlas, and J. Shi, "Proximity-induced ferromagnetism in graphene revealed by the anomalous hall effect," *Phys. Rev. Lett.*, vol. 114, no. 1, 2015.
[30] P. Wei *et al.*, "Strong interfacial exchange field in the graphene/EuS heterostructure," *Nat. Mater.*, vol. 15, no. 7, pp. 711–716, Jul. 2016.
[31] Q. L. He *et al.*, "Tailoring exchange couplings in magnetic topological-insulator/antiferromagnet heterostructures," *Nat. Mater.*, vol. 16, no. 1, pp. 94–100, Jan. 2017.
[32] A. I. Snow, "Magnetic Moment Orientation and Thermal Expansion of Antiferromagnetic CrSb," *Rev. Mod. Phys.*, vol. 25, no. 1, pp. 127–127, Jan. 1953.
[33] H. Wang, P. Bencok, P. Steadman, E. Longhi, J. Zhu, and Z. Wang, "Complete polarization analysis of an APPLE II undulator using a soft X-ray polarimeter," *J. Synchrotron Radiat.*, vol. 19, no. 6, pp. 944–948, Nov. 2012.
[34] G. van der Laan and A. I. Figueroa, "X-ray magnetic circular dichroism - A versatile tool to study magnetism," *Coord. Chem. Rev.*, vol. 277, pp. 95–129, 2014.
[35] C. T. Chen *et al.*, "Experimental confirmation of the x-ray magnetic circular dichroism sum rules for iron and cobalt," 1995.
[36] B.-G. Liu, "Robust half-metallic ferromagnetism in zinc-blende CrSb," *Phys. Rev. B*, vol. 67, no. 17, p. 172411, May 2003.
[37] M. Y. Zhuravlev, E. Y. Tsymbal, and S. S. Jaswal, "Exchange model for oscillatory interlayer coupling and induced unidirectional anisotropy in [Pt/Co]3/NiO/[Pt/Co]3 multilayers," *Phys. Rev. Lett.*, vol. 92, no. 21, pp. 219703–219701, May 2004.
[38] Q. L. He *et al.*, "Topological Transitions Induced by Antiferromagnetism in a Thin-Film Topological Insulator," *Phys. Rev. Lett.*, vol. 121, no. 9, p. 096802, Aug. 2018.

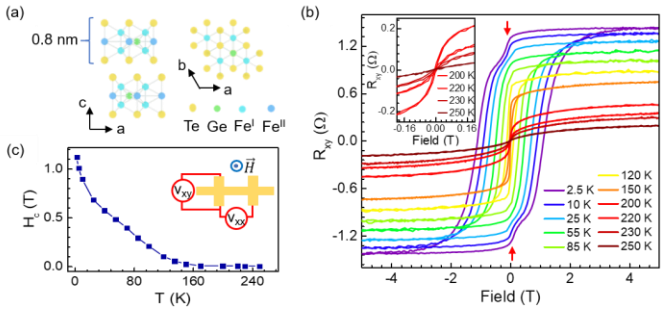

Fig. 1. Ferromagnetism in (1.6 nm CrSb/3.2 nm $Fe_3GeTe_2)_6$ superlattices probed by transport measurement via anomalous Hall effect (AHE). (a) Schematic of lattice structure of Fe_3GeTe_2, in which the left panel is the view along b-axis and right panel is the view along c-axis. The inequivalent sites Fe^{I} and Fe^{II} are distinguished by light and dark blue, respectively. (b) Temperature dependent Hall resistance (R_{xy}) versus magnetic field measured with elevated temperature ranging from 2.5 K to 250 K. The double-switching features at 2.5 K are marked by red arrows. Inset: the partial enlarge diagram in the low field region at 200-250 K, in which H_c reduced to ~3 mT at 230 K and vanished at 250 K. (c) Coercive field (H_c) as a function of temperature (T). Inset: the experimental set-up of transport measurement.

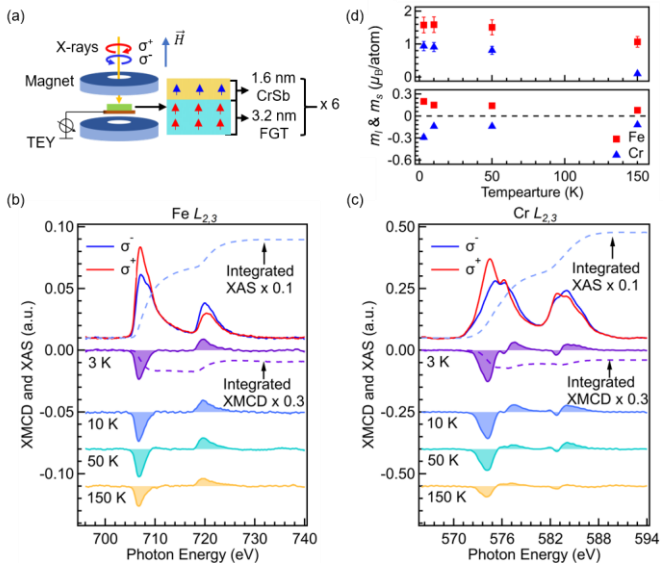

Fig. 2. Element-specific magnetic states measured by XAS and XMCD of (1.6 nm CrSb/3.2 nm $Fe_3GeTe_2)_6$ superlattices. (a) Schematic of experimental setup of XMCD measurement. Inset: the spin configuration of one period (CrSb/Fe_3GeTe_2) superlattices, in which the blue arrows represent the net magnetization of CrSb layers and red arrows represent the magnetization of Fe_3GeTe_2 layers. (b, c) Typical pair of XAS and XMCD spectra at (b) Fe and (c) Cr $L_{2,3}$ edge obtained using TEY mode at 3 K and 5 T with their integrals and that at elevated temperature ranging from 3 K to 150 K (XAS and XMCD spectra are offset vertically for clarity). The dash lines indicate the integration of the spectra. (d) Spin (m_s) (top) and orbital (m_l) (bottom) moments of the Fe (red) and Cr (blue) versus temperature from 3 K to 150 K.

TABLE I
The summary of spin, orbital, and total magnetic moments of Fe_3GeTe_2 systems of our samples, and those reported in literatures.

System	Method	Fe m_s (μ_B/atom)	Fe m_{orb} (μ_B/atom)	Fe m_{total} (μ_B/atom)	m_{orb}/m_s	Ref.
(1.6 nm CrSb/3.2 nm $Fe_3GeTe_2)_6/Al_2O_3$ (0001)	XMCD	1.58 ± 0.2	0.22 ± 0.04	1.8	0.14	[*]
Bulk $Fe_{2.9}GeTe_2$	Neutron powder diffraction	-	-	1.8	-	24
	SQUID-VSM (in-plane)	--	-	1.0	-	
Bulk Fe_3GeTe_2	SQUID-VSM	-	-	1.63	-	15
Bulk Fe_3GeTe_2	XMCD	1.48	0.1	1.58	0.07	19
Bulk Fe_3GeTe_2	SQUID-VSM	-	-	1.37	-	22
Bulk $Fe_{2.97}GeTe_2$	SQUID-VSM	-	-	1.31	-	16
Bulk $Fe_{2.76}GeTe_2$	Neutron diffraction	-	-	1.11	-	
Bulk Fe_3GeTe_2	SQUID-VSM	-	-	1.2	-	14
Bulk Fe_3GeTe_2	SQUID-VSM	-	-	1.2	-	17
Bulk Fe_3GeTe_2	SQUID-VSM	-	-	1.08	-	25
Bulk $Fe_{2.64}GeTe_2$	SQUID-VSM	-	-	1.03	-	23
8 nm Fe_3GeTe_2/Al_2O_3 (0001)	SQUID-VSM	-	-	1.23	-	21
(1.6 nm CrSb/3.2 nm $Fe_3GeTe_2)_3/Al_2O_3$ (0001)	XMCD	1.05 ± 0.1	0.16 ± 0.02	1.21	0.15	26
Bulk Fe_3GeTe_2 (Theory)	LDA+DMFT	1.58	0.063	1.64	0.04	19
Bulk Fe_3GeTe_2 (Theory)	LDA	-	-	1.57	-	27
Bulk Fe_3GeTe_2 (Theory)	LDA+U	-	-	1.48	-	18

[*]: This work